
This is an electronic reprint of the original article.
This reprint may differ from the original in pagination and typographic detail.

Kataja, Mikko; van Dijken, Sebastiaan

Magneto-optical Kerr effect susceptometer for the analysis of magnetic domain wall dynamics

Published in:
Review of Scientific Instruments

DOI:
[10.1063/1.3647313](https://doi.org/10.1063/1.3647313)

Published: 01/01/2011

Document Version
Publisher's PDF, also known as Version of record

Please cite the original version:
Kataja, M., & van Dijken, S. (2011). Magneto-optical Kerr effect susceptometer for the analysis of magnetic domain wall dynamics. *Review of Scientific Instruments*, 82(10), Article 103901.
<https://doi.org/10.1063/1.3647313>

This material is protected by copyright and other intellectual property rights, and duplication or sale of all or part of any of the repository collections is not permitted, except that material may be duplicated by you for your research use or educational purposes in electronic or print form. You must obtain permission for any other use. Electronic or print copies may not be offered, whether for sale or otherwise to anyone who is not an authorised user.

Magneto-optical Kerr effect susceptometer for the analysis of magnetic domain wall dynamics

Mikko Kataja, and Sebastiaan van Dijken

Citation: [Review of Scientific Instruments](#) **82**, 103901 (2011); doi: 10.1063/1.3647313

View online: <https://doi.org/10.1063/1.3647313>

View Table of Contents: <http://aip.scitation.org/toc/rsi/82/10>

Published by the [American Institute of Physics](#)

Articles you may be interested in

[Surface magneto-optic Kerr effect](#)

[Review of Scientific Instruments](#) **71**, 1243 (2000); 10.1063/1.1150496

[The motion of 180° domain walls in uniform dc magnetic fields](#)

[Journal of Applied Physics](#) **45**, 5406 (1974); 10.1063/1.1663252

[Perpendicular magnetic anisotropy and magnetic domain structure in sputtered epitaxial FePt \(001\) L₁0 films](#)

[Journal of Applied Physics](#) **84**, 5686 (1998); 10.1063/1.368831

[Controlling the size and relaxation dynamics of superferromagnetic domains](#)

[Journal of Applied Physics](#) **117**, 153907 (2015); 10.1063/1.4918670

[Direct imaging of the magnetization reversal in microwires using all-MOKE microscopy](#)

[Review of Scientific Instruments](#) **85**, 103702 (2014); 10.1063/1.4896758

[Vectorial Kerr magnetometer for simultaneous and quantitative measurements of the in-plane magnetization components](#)

[Review of Scientific Instruments](#) **85**, 053904 (2014); 10.1063/1.4871098

PHYSICS TODAY

WHITEPAPERS

MANAGER'S GUIDE

Accelerate R&D with
Multiphysics Simulation

READ NOW

PRESENTED BY
 COMSOL

Magneto-optical Kerr effect susceptometer for the analysis of magnetic domain wall dynamics

Mikko Kataja and Sebastiaan van Dijken^{a)}

NanoSpin, Department of Applied Physics, Aalto University School of Science, P.O. Box 15100, FI-00076 Aalto, Finland

(Received 29 August 2011; accepted 13 September 2011; published online 14 October 2011)

Domain wall dynamics in thin magnetic films with perpendicular and in-plane anisotropy is studied using a novel magneto-optical Kerr effect susceptometry method. The method allows for measurements of domain wall motion under ac field excitation and the analysis of dynamic modes as a function of driving frequency and magnetic field amplitude. Domain wall dynamics in the perpendicular anisotropy system, a Co/Pt multilayer, is characterized by thermally activated creep motion. For this dynamic mode, a polydispersivity exponent of $\beta = 0.50 \pm 0.03$ is derived at small excitation energy, which is in excellent agreement with theoretical models. The dynamics of the other system, a Co wire with transverse uniaxial anisotropy, is dominated by viscous slide motion in a regular magnetic stripe pattern. Analytical expressions are derived for this magnetic configuration and by using these expressions, accurate values for the depinning field and the domain wall mobility are extracted from the susceptibility measurements. © 2011 American Institute of Physics. [doi:10.1063/1.3647313]

I. INTRODUCTION

Domain wall motion is one of the key magnetization reversal processes in magnetic materials and forms the basis of several concepts for memory¹ and logic² devices. Domain walls can be driven by an external magnetic field or spin-polarized current and, depending on the magnitude of the driving force, distinctive modes of wall motion can be activated.^{3–8} Motion at the low energy side of the excitation spectrum is known as creep. This is a thermally activated state, which is characterized by small wall velocity and considerable wall roughness. A transition to viscous slide motion occurs when the driving force exceeds the depinning strength. In this case, the wall velocity is proportional to the external field via the domain wall mobility, which in turn depends on internal wall dynamics as predicted by theoretical models^{9–11} and confirmed by experiments on magnetic nanowires.^{12–15} In most studies, the motion of domain walls is analyzed using magnetic field or current pulses. A less explored feature of magnetic domain walls is their dynamic response in alternating fields. Under ac excitation ($H = H_0 \cos \omega t$), both domain wall creep and slide can be activated and this results in distinctive dynamic modes which not only depend on field amplitude but also vary with driving frequency.^{16–19} Moreover, additional states such as domain wall relaxation at low frequency/small fields and magnetic switching at fields exceeding the coercivity ($H_0 > H_c$) may appear in ac spectra. Detailed investigations of these dynamic modes are relevant to potential applications based on magnetic domain wall motion and, as they represent a more generic feature of ac-driven elastic interfaces in weakly disordered media, might also provide insight into the dynamics of other physical systems. Related examples include domain walls in ferroelectric materials,^{19,20}

vortices in superconductors,⁵ and charge density waves in materials with a highly anisotropic band structure.²¹

Magneto-optical Kerr effect susceptometry is a versatile tool in modern magnetic materials research. This ac technique, which combines ease of implementation, low cost, and high sensitivity, has been utilized in studies on magnetic phase transitions^{22–24} and magnetic domain responses^{25,26} in thin and ultra-thin magnetic films. Moreover, it has been shown that the imaginary Kerr signal provides additional information on energy absorption in magnetic systems.^{26,27} Here, we extend the use of magneto-optical Kerr effect susceptometry to direct probing of domain wall dynamics in alternating driving fields. The setup allows for low-noise measurements of the complex Kerr signal ($V_{Kerr} = X - iY$) as a function of field amplitude (H_0) and driving frequency ($f = \omega/2\pi$). Because the measurement signal is directly proportional to the magnetic susceptibility ($V_{Kerr} \sim \chi H_0$), it contains all its characteristic spectral signatures.^{17–19} This is most apparent when the data is plotted in the Cole-Cole representation (Y vs. X).²⁸ In this case, the distinctive dynamic modes are indicated by well-defined linear and circular segments as schematically illustrated in Fig. 1. A Cole-Cole plot of the Kerr signal can therefore be considered as the fingerprint of domain wall dynamics in magnetic thin films. In addition to a qualitative analysis of dynamic modes and phase transitions, the magneto-optical Kerr effect susceptometer can also be used to extract important physical parameters. Using two magnetic samples with different anisotropy configurations, we demonstrate that the polydispersivity exponent of domain wall creep (β), the depinning field for slide motion (H_d), and the domain wall mobility (μ_w) can be determined.

II. EXPERIMENT AND SAMPLES

The magneto-optical Kerr effect susceptometer consists of a HeNe laser, polarizing optics (Glan-Thompson prisms

^{a)} Author to whom correspondence should be addressed. Electronic mail: sebastiaan.van.dijken@aalto.fi.

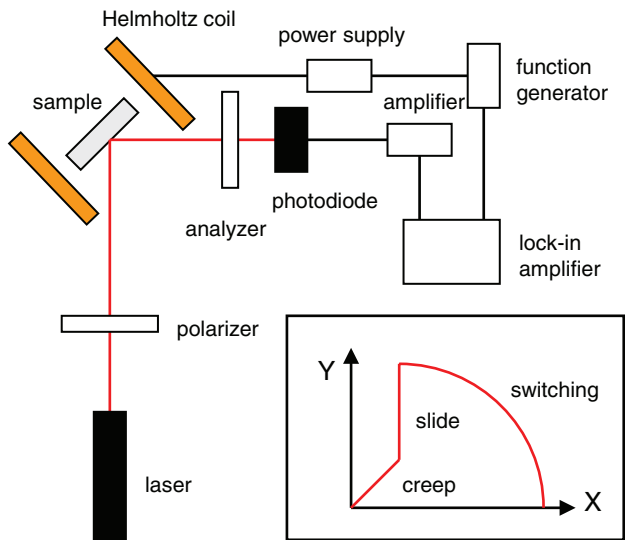


FIG. 1. (Color online) Schematic illustration of the magneto-optical Kerr effect susceptometer and the dynamic creep, slide, and switching modes in a Cole-Cole plot.

with an extinction ratio of 5×10^{-6} , a high-speed silicon photodiode, a variable gain low-noise current amplifier (Femto DLPCA-200), and a lock-in amplifier (Stanford Research Systems SR830 DSP). The ac magnetic field is generated by a water-cooled Helmholtz coil with a low inductance of $23 \mu\text{H}$. The coil is driven by a Kepco power supply and a function generator and the maximum field amplitude amounts 14.4 mT . Rotation of the Helmholtz coil allows for the application of in-plane and out-of-plane magnetic fields. The driving frequency can be varied by more than four orders of magnitude from 0.5 Hz to about 10 kHz . The Kerr signal (V_{Kerr}) is measured by current-to-voltage conversion with a gain of $G = 10^7 \text{ V/A}$ and lock-in amplification of the photodiode output. The photodiode has a responsivity of about 0.35 A/W . In the experiments, the polarizing optics is set to an angle of $\theta \approx 2^\circ$ from extinction, which, together with the other experimental conditions, produces a noise level of $\leq 0.5 \mu\text{V}$ in the entire frequency range.

For an arbitrary magnetization reversal process, the measurement signal can consist of longitudinal, transverse, and polar Kerr components.²⁹ If, however, the magnetization is aligned along a single axis by uniaxial magnetic anisotropy, one specific Kerr configuration can be selected. In the case of pure polar or longitudinal effects, the Kerr signal is linearly proportional to the magnetization component along the applied field direction, i.e.,

$$V_{Kerr}(t) = rM(t) + K. \quad (1)$$

Here, r and K are constants that depend on the magneto-optical response of the sample, the polarizer and analyzer angles, and the amplification settings. For ac magnetic fields ($H = H_0 \cos \omega t$), both $M(t)$ and $V_{Kerr}(t)$ are periodic functions and, hence, they can be written as Fourier series. The lock-in amplifier measures the first Fourier component of the Kerr signal, which for the in-phase and out-of-phase components are

given by

$$X = \frac{r}{\pi/\omega} \int_{-\pi/\omega}^{\pi/\omega} V_{Kerr}(t) \cos(\omega t) dt, \quad (2)$$

$$Y = \frac{r}{\pi/\omega} \int_{-\pi/\omega}^{\pi/\omega} V_{Kerr}(t) \sin(\omega t) dt. \quad (3)$$

Prior to the Kerr effect susceptibility measurements, a magnetic domain pattern is generated using a demagnetization process. The dynamics of the magnetic domain walls is subsequently analyzed by recording the X and Y signals at constant magnetic field amplitude (H_0). During these measurements the driving frequency is decreased in steps, typically from 10 kHz to 1 Hz . Plots of the data in Cole-Cole representation (Y vs. X) immediately reflect the active dynamic modes under the selected experimental conditions. This procedure is repeated for other H_0 . A separate Kerr magnetometer and Kerr microscope (Evico) are used to measure quasi-static magnetic hysteresis curves and to image the magnetic domain pattern after the demagnetization process.

To test the magneto-optical Kerr effect susceptometry method, we used two samples. The first is a $2 \text{ nm Pt}/[0.4 \text{ nm Co}/2 \text{ nm Pt}]_5$ multilayer with perpendicular magnetic anisotropy. This multilayer was grown on a Si/SiO_2 substrate by magnetron sputtering at room temperature. The second sample is a 40 nm thick and $400 \mu\text{m}$ wide Co wire with a transverse growth-induced uniaxial magnetic easy axis. The Co film was deposited by electron-beam evaporation and the wire was patterned using photolithography and lift-off.

III. ANALYSIS

A. Domain wall creep

Figure 2 summarizes the results for the $2 \text{ nm Pt}/[0.4 \text{ nm Co}/2 \text{ nm Pt}]_5$ multilayer with perpendicular magnetic anisotropy. The demagnetization process results in an irregular domain pattern as illustrated by the Kerr microscopy image. This type of domain structure balances exchange, anisotropy, and dipolar energies in perpendicular magnetic systems.^{30,31} The size of the domains ranges from about 1 to $5 \mu\text{m}$. The magnetization reversal process in a slowly varying magnetic field is rather gradual and proceeds by inverse domain nucleation and relatively slow domain wall motion. The quasi-static magnetic hysteresis curve in Fig. 2(b) indicates that the reversal process commences at an applied field of 6 mT and that the magnetization saturates at about 10 mT .

The active dynamic modes in this sample are analyzed using the magneto-optical Kerr effect susceptometer. In these measurements the demagnetized state, which is shown in Fig. 2(a), is used as starting point. Contrary to magnetic hysteresis, domain nucleation is therefore not required to initiate a magnetic response. In the susceptibility experiments, a signal is measured when the out-of-plane ac magnetic field thermally activates back and forth motion of the existing domain walls. The Cole-Cole plots in Figs. 2(c) and 2(d) summarize the results for different magnetic field amplitudes. At high driving frequencies, the domain walls remain pinned and

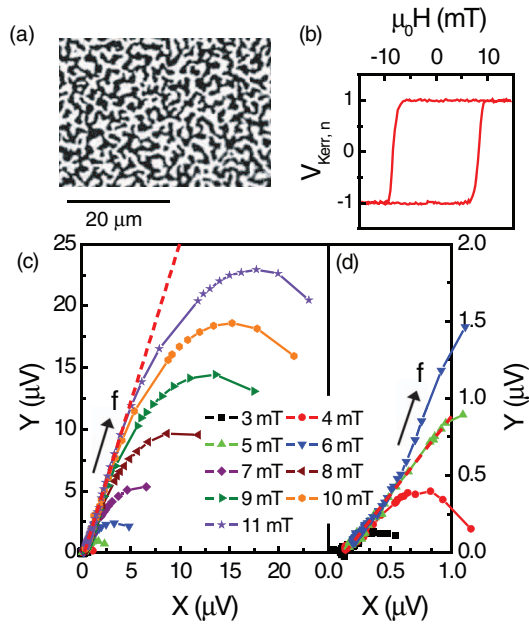


FIG. 2. (Color online) Kerr microscopy image of the demagnetized domain pattern (a), quasi-static magnetic hysteresis curve (b), and Cole-Cole plots of the complex Kerr signal for different field amplitudes (c, d) measured on the 2 nm Pt/[0.4 nm Co/2 nm Pt]₅ sample. The arrows in the Cole-Cole plots indicate the data collection sequence, which starts at high- and ends at low driving frequency. The dashed red lines in (c, d) are linear fits to the experimental susceptibility data.

$X = Y = 0$. Both the in-phase and out-of-phase components of the Kerr signal start to increase when the frequency is decreased. The initial slope of the Y vs. X curves is 1 (Fig. 2(d)), but at lower frequency and higher field amplitude it increases to about 2.5 (Fig. 2(c)). The change in slope signifies a gradual transition from thermally activated domain wall creep to slide-like motion with lower domain wall resistance. Pure viscous domain wall slide, however, would result in a fully imaginary signal which is not observed for this sample. The main reason for this is the large lateral variation in perpendicular anisotropy strength due to small but significant thickness variations in the thin Co layers. This produces a high density of domain wall pinning sites with a large distribution of pinning strengths and, as a result, a gradual magnetization reversal process. Pure slide motion in such disordered samples requires an applied magnetic field that well-exceeds the depinning field for domain wall motion as illustrated by experiments using ultrafast magnetic field pulses.^{6,8} In our ac-driven measurements, the dynamic range is limited by a transition from slide-like motion to full magnetization reversal. In the Cole-Cole plots, this transition is indicated by a change in the shape of the curve from linear at high frequencies to circular at low frequencies.

For the 2 nm Pt/[0.4 nm Co/2 nm Pt]₅ multilayer, thermally activated creep motion at the low energy side of the excitation spectrum, i.e., for small field amplitude, can be analyzed in more detail. In this dynamic regime, the complex Kerr signal can be written as¹⁷⁻¹⁹

$$V_{Kerr}(\omega) = V_{\infty}(1 + (i\omega\tau)^{-\beta}) = X - iY. \quad (4)$$

Here, β is an empirical polydispersivity exponent, τ is a characteristic relaxation time, and V_{∞} is the limiting Kerr signal for $\omega \rightarrow \infty$. From theoretical models,³⁻⁵ it can be derived that the creep exponent satisfies the relationship $\beta = (2 - 2\zeta)/z$,¹⁸ where the exponent ζ is an indication of the domain wall roughness and the exponent z describes the dynamic response of a domain wall in an applied magnetic field. For a one-dimensional wall in a two-dimensional thin magnetic film, the theoretical values are $\zeta = 2/3$ (Refs. 3-5) and $z \approx 4/3$ (Ref. 32) and, thus, $\beta \approx 0.5$. For an analysis of the Cole-Cole plots, Eq. (4) can easily be transformed into the following linear function:

$$Y = (X - V_{\infty}) \tan(\pi\beta/2). \quad (5)$$

The slope of a Cole-Cole plot in the dynamic slide regime thus equals $\tan(\pi\beta/2)$. Our experimental data on the 2 nm Pt/[0.4 nm Co/2 nm Pt]₅ sample indicates a slope of 1 ± 0.1 at small field amplitude and high frequency (Fig. 2(d)) and we therefore obtain $\beta = 0.50 \pm 0.03$, in good agreement with theoretical models.

B. Domain wall slide

The magnetic domain structure in the 40 nm thick and 400 μm wide Co wire after demagnetization is shown in Fig. 3(a). In this sample, a regular stripe pattern with 180° domain walls forms. The magnetization aligns along the growth-induced uniaxial magnetic easy axis, i.e., transverse to the wire axis. Magnetization reversal in this sample is much more abrupt than in the 2 nm Pt/[0.4 nm Co/2 nm Pt]₅ multilayer as illustrated by the quasi-static magnetic hysteresis curve in Fig. 3(b). The application of an ac magnetic field parallel to the uniaxial magnetic easy axis results in alternating sideways motion of the magnetic domain walls. The dynamic response as measured by the magneto-optical Kerr effect susceptometer is summarized in Fig. 3(c). For small field amplitudes just above the depinning field, the motion of the walls still contains a resistive component. The slope of the Cole-Cole plots at high frequencies, however, increases rapidly when the field amplitude is increased and the Kerr signals become fully imaginary. The vertical segments of the curves in Fig. 3(c) clearly indicate viscous slide motion without any domain wall resistance. The imaginary Kerr signals from this sample are the magnetic equivalent of the imaginary permittivity of superconducting currents. As the driving frequency is decreased in steps, the sideways motion of the walls, and thus the imaginary Kerr signal, increase. Once the walls move about half the domain width away from their zero-field equilibrium position, the domains coalesce and the magnetization of the wire saturates. A further reduction of the driving frequency therefore results in full magnetic switching. The transition from domain wall slide to magnetic switching is abrupt as indicated by the near-instant change in the shape of the Cole-Cole plot from a vertical to a quarter circle segment.

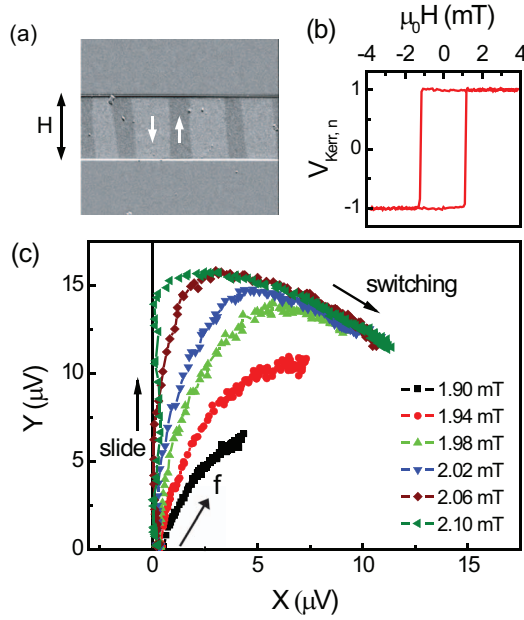


FIG. 3. (Color online) Kerr microscopy image of the demagnetized domain pattern (a), quasi-static magnetic hysteresis curve (b), and Cole-Cole plots of the complex Kerr signal for different field amplitudes (c) measured on the 40 nm thick and 400 μm wide Co wire. The arrows in (a) indicate the magnetic field direction and orientation of the film magnetization and the arrows in (c) label the active dynamic modes and the driving frequency (from high to low).

For sideways domain wall slide in a regular magnetic stripe pattern, a more quantitative analysis is possible. Below we derive an expression that can be used to extract the depinning field (H_d) and the domain wall mobility (μ_w) from Kerr susceptibility data. In the slide regime, the domain wall velocity is proportional to the applied magnetic field via the

domain wall mobility^{9–11}

$$\dot{x}(t) = \mu_w H(t). \quad (6)$$

However, domain wall slide is only activated when the alternating magnetic field ($H(t) = H_0 \cos(\omega t)$) exceeds the depinning field H_d . As a result, an effective field $H_{eff}(t)$ drives the domain walls during certain periods of the ac field cycle. The effective field is given by

$$H_{eff}(t) = \begin{cases} H_0 \cos(\omega t) - H_d & \text{if } H_0 \cos(\omega t) \geq H_d \\ H_0 \cos(\omega t) + H_d & \text{if } H_0 \cos(\omega t) \leq -H_d \\ 0 & \text{otherwise} \end{cases}. \quad (7)$$

For regular magnetic stripe patterns with an average domain width D (see Fig. 4), the time evolution of the magnetization ($M(t)$) can be written as

$$\frac{M(t)}{M_s} = \frac{2}{D} x(t), \quad (8)$$

where M_s is the saturation magnetization. By inserting Eq. (6) into Eq. (8) one obtains the rate equation

$$\frac{dM}{dt} = \frac{2M_s \mu_w}{D} H_{eff}(t). \quad (9)$$

The time evolution of the magnetization is therefore given by the following integral:

$$M(t) = \frac{2M_s \mu_w}{D} \int_0^t H_{eff}(t) dt. \quad (10)$$

This integral can be analytically solved and the solution is divided into five expressions for different periods of the ac field cycle

$$M(t) = \frac{2M_s \mu_w}{D} \begin{cases} \frac{H_0}{\omega} \sin(\omega t) - H_d t & t \in [2\pi n/\omega, (t_0 + 2\pi n)/\omega], \\ \frac{H_0}{\omega} \sqrt{1 - \left(\frac{H_d}{H_0}\right)^2} - H_d \frac{t_0}{\omega} & t \in [(t_0 + 2\pi n)/\omega, (\pi - t_0 + 2\pi n)/\omega], \\ \frac{H_0}{\omega} \sin(\omega t) + H_d \left(t - \frac{\pi}{\omega}\right) & t \in [(\pi - t_0 + 2\pi n)/\omega, (\pi + t_0 + 2\pi n)/\omega], \\ -\frac{H_0}{\omega} \sqrt{1 - \left(\frac{H_d}{H_0}\right)^2} + H_d \frac{t_0}{\omega} & t \in [(\pi + t_0 + 2\pi n)/\omega, (2\pi(n+1) - t_0)/\omega], \\ \frac{H_0}{\omega} \sin(\omega t) + H_d \left(\frac{2\pi}{\omega} - t\right) & t \in [(2\pi(n+1) - t_0)/\omega, 2\pi(n+1)/\omega]. \end{cases} \quad (11)$$

Here, $t_0 = \cos^{-1}(H_d/H_0)$. The time evolution of $M(t)$ for $H_0/H_d = 1.2$ is shown as an example in Fig. 4. As described in Sec. II, the pure longitudinal Kerr signal from this sample is linearly proportional to the film magnetization. Consequently, inserting Eq. (11) into Eqs. (1)–(3) gives the expressions for the in-phase and out-of-phase components of the imaginary Kerr signal. The results are

$$X = 0, \quad (12)$$

$$Y = r \frac{2M_s \mu_w}{D} \frac{2}{\pi \omega} (H_0 t_0 - H_d \sqrt{1 - (H_d/H_0)^2}), \quad (13)$$

which confirms that pure sideways slide motion only produces an imaginary measurement signal. The factor r can be eliminated by normalizing Y to the maximum Kerr signal (V_{max}) that is obtained for reversible switching between two fully saturated states. In this case, V_{max} is given by a block wave with a peak-to-peak amplitude of $2M_s$. The quantity measured by

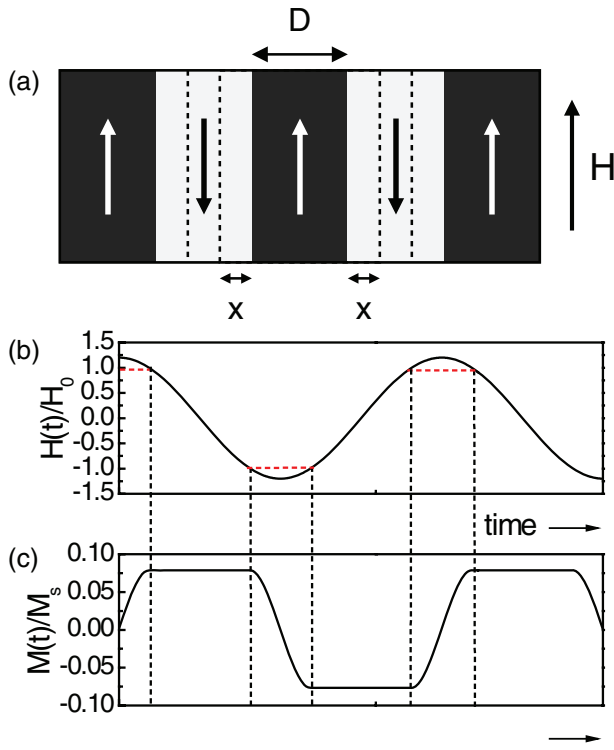


FIG. 4. (Color online) Schematic illustration of sideways domain wall motion in a regular magnetic stripe pattern (a) and corresponding time evolution of the normalized film magnetization (c) for an applied ac magnetic field ($H = H_0 \cos \omega t$) with $H_0/H_d = 1.2$ (b).

the lock-in amplifier for such a signal is

$$V_{\max} = r \frac{4}{\pi} M_s. \quad (14)$$

Thus, the normalized imaginary signal ($Y_n = Y/V_{\max}$) is given by

$$Y_n = \frac{1}{f} \frac{1}{2\pi D} \mu_w (H_0 t_0 - H_d \sqrt{1 - (H_d/H_0)^2}), \quad (15)$$

where ω is replaced by $2\pi f$. This result is exact, but can be simplified by considering $\cos(t_0) \approx 1 - t_0^2/2$ for small t_0 , which gives $t_0 \approx \sqrt{2} \sqrt{1 - H_d/H_0}$. Another approximation for $H_d/H_0 \approx 1$ gives $\sqrt{1 - (H_d/H_0)^2} = \sqrt{(1 - H_d/H_0)(1 + H_d/H_0)} \approx \sqrt{2} \sqrt{1 - H_d/H_0}$. Using both approximations, the normalized imaginary Kerr signal can be written as

$$Y_n = \frac{1}{f} \frac{1}{\sqrt{2}\pi D} \mu_w (H_0 - H_d) \sqrt{1 - H_d/H_0} = \frac{1}{f} T(H_0). \quad (16)$$

This expression can be used to extract H_d and μ_w from the experimental data. The left panel of Fig. 5 shows plots of Y_n as a function of $1/f$ for different field amplitudes H_0 . The slope of the linear fits to these curves ($T(H_0)$) are plotted versus magnetic field amplitude in the right panel. The solid red line in this graph is a fit to the data using Eq. (16). From this fit and Kerr microscopy images indicating an average domain size of $D = 230 \mu\text{m}$, a depinning field of $\mu_0 H_d$

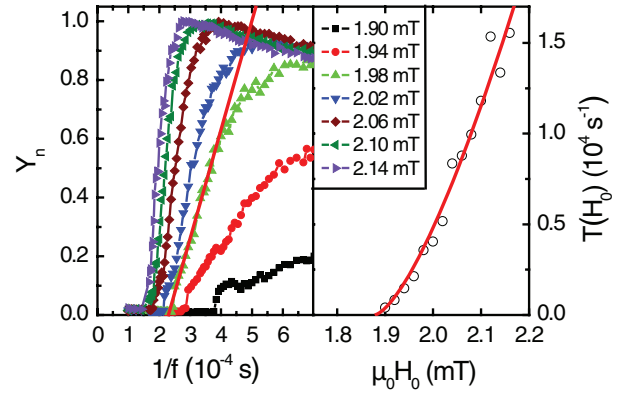


FIG. 5. (Color online) Normalized out-of-phase Kerr signal Y_n as a function of the inverse driving frequency $1/f$. In the right panel, the slope of the Y_n versus $1/f$ curve is plotted for different applied field amplitudes. The solid red line is a fit to the data using Eq. (16).

$= 1.88 \text{ mT}$, and a domain wall mobility of $\mu_w = 0.19 \text{ m}^2 \text{s}^{-1} \text{A}^{-1}$ (or $15 \text{ ms}^{-1} \text{Oe}^{-1}$) are derived.

The error in this quantitative analysis contains three main components. First, fluctuations in the laser intensity, sample vibrations, and noise in the photodiode produce an error in the Kerr signal. The total noise, however, is relatively small ($\leq 0.5 \mu\text{V}$) and, thus, the experimental setup only introduces a small error in $\mu_0 H_d$ and μ_w . From the data in Fig. 5, an error of $\pm 5\%$ is inferred. The two approximations that are used to simplify Eq. (15) into Eq. (16) also introduce an uncertainty. In our experiments, the smallest H_d/H_0 ratio is 0.88 and under these conditions the total error from the two approximations is negligible ($< 3\%$). However, for smaller H_d/H_0 the error increases significantly and the exact solution of Eq. (15) should be used to extract accurate results. A third source of error is the variation in D . In our Co wire, the average domain wall width is $230 \pm 140 \mu\text{m}$ and thus the error ε_D is about 60%. In the magneto-optical Kerr effect susceptometer, the average number of domains under study (n) is given by the ratio between the size of the laser spot on the magnetic wire (L) and D . Consequently, the error in μ_w (ε_μ) that is introduced by variations in D scales with $1/\sqrt{n}$ and thus

$$\varepsilon_\mu = \varepsilon_D \sqrt{\frac{D}{L}}. \quad (17)$$

In our setup, $L \approx 1.5 \text{ mm}$ which gives an approximate error of 23% in the derived mobility for domain wall slide, i.e., $\mu_w = 0.19 \pm 0.04 \text{ m}^2 \text{s}^{-1} \text{A}^{-1}$ (or $15 \pm 3 \text{ ms}^{-1} \text{Oe}^{-1}$). Equation (17) clearly illustrates that the magneto-optical Kerr effect susceptometry method produces accurate domain wall mobility values when the width of the domains is uniform or when $D \ll L$. We note that the error in the depinning field ($\mu_0 H_d$) is considerably smaller than ε_μ because it does not critically depend on ε_D . Instead, it is determined by the onset of domain wall motion and this can accurately be extracted from the right panel in Fig. 5.

In a well-established one-dimensional model of domain wall dynamics,^{9,11} the domain wall mobility is given by $\mu_w = \gamma \Delta / \alpha$, where γ is the gyromagnetic ratio, Δ is the domain wall width, and α is the Gilbert damping parameter.

Here, we use this expression to estimate theoretically the domain wall mobility in the 40-nm thick Co wire. Measurements on other Co wires indicate a rapid increase of μ_w for a film thickness (t) below about 50 nm.³³ This change in wall mobility signals a transition from a Bloch-type domain wall above the critical thickness $t_c \approx 50$ nm to a Néel wall at $t < 50$ nm.³⁴ For films with $t \approx t_c$, the width of the domain wall is approximately $\Delta \approx t_c$ and for $t < t_c$ the width of the Néel wall monotonically increases with decreasing film thickness.³⁵ Thus, for domain walls in the 40-nm thick Co wire, $\Delta \geq 50$ nm. The Gilbert damping parameter in the Co film was independently measured by pulse-inductive microwave magnetometry (PIMM).³⁶ Using the result, $\alpha = 0.01$, together with $\Delta = 50$ nm and $\gamma = 3.52 \times 10^4 \text{ ms}^{-1} \text{ A}^{-1}$ gives $\mu_w = 0.18 \text{ m}^2 \text{ s}^{-1} \text{ A}^{-1}$, which is well within the error margin of the experimental result.

IV. CONCLUSIONS

A novel method based on magneto-optical Kerr effect susceptometry was demonstrated for fast qualitative and quantitative analysis of domain wall dynamics in thin magnetic films. Measurements of the in-phase and out-of-phase components of the complex Kerr signal during ac field excitation directly reveal the active dynamic modes and phase transitions as a function of driving frequency and field amplitude. Moreover, the polydispersivity exponent of domain wall creep can accurately be extracted for thermally activated domain wall motion. Finally, it was shown that regular magnetic stripe patterns could be used to determine accurately the depinning field and domain wall mobility for viscous slide motion. The accuracy of this method depends on the regularity of the stripe pattern and the average distance between the domain walls.

ACKNOWLEDGMENTS

This work was supported in part by Academy of Finland (Grant No. 127731). We thank T. H. E. Lahtinen and Q. H. Qin for the preparation of the Co wire and assistance with the Kerr microscope.

¹S. S. P. Parkin, M. Hayashi, and L. Thomas, *Science* **320**, 190 (2008).

²D. A. Allwood, G. Xiong, C. C. Faulkner, D. Atkinson, D. Petit, and R. P. Cowburn, *Science* **309**, 1688 (2005).

³M. V. Feigel'man, V. B. Geshkenbein, A. I. Larkin, and V. M. Vinokur, *Phys. Rev. Lett.* **63**, 2303 (1989).

⁴T. Nattermann, Y. Shapir, and I. Vilfan, *Phys. Rev. B* **42**, 8577 (1990).

⁵G. Blatter, M. V. Feigel'man, V. B. Geshkenbein, A. I. Larkin, and V. M. Vinokur, *Rev. Mod. Phys.* **66**, 1125 (1994).

⁶S. Lemerle, J. Ferré, C. Chappert, V. Mathet, T. Giamarchi, and P. Le Doussal, *Phys. Rev. Lett.* **80**, 849 (1998).

⁷P. Chauve, T. Giamarchi, and P. Le Doussal, *Phys. Rev. B* **62**, 6241 (2000).

⁸P. J. Metaxas, J. P. Jamet, A. Mougin, M. Cormier, J. Ferré, V. Baltz, B. Rodmacq, B. Dieny, and R. L. Stamps, *Phys. Rev. Lett.* **99**, 217208 (2007).

⁹N. L. Schryer and L. R. Walker, *J. Appl. Phys.* **45**, 5406 (1974).

¹⁰J. C. Slonczewski, *Int. J. Magn.* **2**, 85 (1972).

¹¹A. P. Malozemoff and J. C. Slonczewski, *Magnetic Domain Walls in Bubble Materials* (Academic, New York, 1979).

¹²G. S. D. Beach, C. Nistor, C. Knutson, M. Tsoi, and J. L. Erskine, *Nature Mater.* **4**, 741 (2005).

¹³G. S. D. Beach, C. Knutson, C. Nistor, M. Tsoi, and J. L. Erskine, *Phys. Rev. Lett.* **97**, 057203 (2006).

¹⁴M. Hayashi, L. Thomas, Y. B. Bazaliy, C. Rettner, R. Moriya, X. Jiang, and S. S. P. Parkin, *Phys. Rev. Lett.* **96**, 197207 (2006).

¹⁵M. Hayashi, L. Thomas, C. Rettner, R. Moriya, and S. S. P. Parkin, *Nat. Phys.* **3**, 21 (2007).

¹⁶T. Nattermann, V. Pokrovsky, and V. M. Vinokur, *Phys. Rev. Lett.* **87**, 197005 (2001).

¹⁷X. Chen, O. Sichel Schmidt, W. Kleemann, O. Petravic, C. Binek, J. B. Sousa, S. Cardoso, and P. P. Freitas, *Phys. Rev. Lett.* **89**, 137203 (2002).

¹⁸W. Kleemann, J. Rhensius, O. Petravic, J. Ferré, J. P. Jamet, and H. Bernas, *Phys. Rev. Lett.* **99**, 097203 (2007).

¹⁹W. Kleemann, *Annu. Rev. Mater. Res.* **37**, 415 (2007).

²⁰T. Braun, W. Kleemann, J. Dec, and P. A. Thomas, *Phys. Rev. Lett.* **94**, 117601 (2005).

²¹G. Grüner, *Rev. Mod. Phys.* **60**, 1129 (1988).

²²A. Berger, S. Knappmann, and H. P. Oepen, *J. Appl. Phys.* **75**, 5598 (1994).

²³W. Wulfhekel, S. Knappmann, and H. P. Oepen, *J. Magn. Magn. Mater.* **163**, 267 (1996).

²⁴G. Garreau, E. Beaurepaire, K. Ounadjela, and M. Farle, *Phys. Rev. B* **53**, 1083 (1996).

²⁵A. Berger, A. W. Pang, and H. Hopster, *Phys. Rev. B* **52**, 1078 (1995).

²⁶P. Pouloupoulos, M. Farle, U. Bovensiepen, and K. Baberschke, *Phys. Rev. B* **55**, R11961 (1997).

²⁷C. S. Arnold, M. Dunlavy, and D. Venus, *Rev. Sci. Instrum.* **68**, 4212 (1997).

²⁸K. S. Cole and R. H. Cole, *J. Chem. Phys.* **9**, 341 (1941).

²⁹Z. Q. Qiu and S. D. Bader, *Rev. Sci. Instrum.* **71**, 1243 (2000).

³⁰A. Hubert and R. Schäfer, *Magnetic Domains: The Analysis of Magnetic Microstructures* (Springer, Heidelberg, 1998).

³¹M. Czapkiewicz, T. Stobiecki, and S. van Dijken, *Phys. Rev. B* **77**, 024416 (2008).

³²T. Nattermann, S. Stepanow, L.-H. Tang, and H. Leschhorn, *J. Phys. II* **2**, 1483 (1992).

³³M. Kataja, "Magneto-Optical Kerr Effect Susceptometer for the Analysis of Magnetic Domain Wall Dynamics," M.S. thesis (Aalto University, 2011).

³⁴V. V. Volkov and V. A. Bokov, *Phys. Solid. State* **50**, 199 (2008).

³⁵R. C. O'Handley, *Modern Magnetic Materials: Principles and Applications* (Wiley, New York, 2000).

³⁶A. B. Kos, T. J. Silva, and P. Kabos, *Rev. Sci. Instrum.* **73**, 3563 (2002).